ANNUAL REVIEWS

Annual Review of Control, Robotics, and Autonomous Systems

From Theoretical Work to Clinical Translation: Progress in Concentric Tube Robots

Zisos Mitros,[1,2] S.M. Hadi Sadati,[1] Ross Henry,[1] Lyndon Da Cruz,[2,3] and Christos Bergeles[1]

[1]Robotics and Vision in Medicine Lab, School of Biomedical Engineering and Imaging Sciences, King's College London, London, United Kingdom; email: smh_sadati@kcl.ac.uk

[2]Wellcome/EPSRC Centre for Interventional and Surgical Sciences, University College London, London, United Kingdom

[3]Moorfields Eye Hospital, London, United Kingdom

Annu. Rev. Control Robot. Auton. Syst. 2022. 5:335–59

First published as a Review in Advance on October 19, 2021

The *Annual Review of Control, Robotics, and Autonomous Systems* is online at control.annualreviews.org

https://doi.org/10.1146/annurev-control-042920-014147

Keywords

concentric tube robots, continuum robots, surgical robots

Abstract

Continuum robots can traverse anatomical pathways to intervene in regions deep inside the human body. They are able to steer along 3D curves in confined spaces and dexterously handle tissues. Concentric tube robots (CTRs) are continuum robots that comprise a series of precurved elastic tubes that can be translated and rotated with respect to each other to control the shape of the robot and tip pose. CTRs are a rapidly maturing technology that has seen extensive research over the past decade. Today, they are being evaluated as tools for a variety of surgical applications, as they can offer precision and manipulability in tight workspaces. This review provides an exhaustive classification of research on CTRs based on their clinical applications and highlights approaches for modeling, control, design, and sensing. Competing approaches are critically presented, leading to a discussion of future directions to address the limitations of current research and its translation to clinical applications.

1. INTRODUCTION

Robot-assisted single-port surgery is envisioned as the next step in minimally invasive surgery, as it offers lower morbidity, improved cosmesis due to the elimination of peripheral ports, reduced trauma, and shorter hospital stays (1). To deliver optimal therapies, especially when deep-seated pathologies are targeted, single-port surgery requires instrumentation with increased dexterity and flexibility to overcome the challenges of confined surgical workspaces and a lack of articulation.

Continuum robots show promise when anatomical pathways need to be traversed, as they are able to reach regions that are inaccessible using conventional rigid robotic or manual instruments, while requiring only a single incision or port. Concentric tube robots (CTRs) (see **Figure 1**), also known as active cannulas, are continuum robots that possess a continuously flexible backbone that comprises concentric precurved tubes made of superelastic material, most commonly nitinol (NiTi). The shape and tip pose of those miniature robotic manipulators are controlled by the relative rotation and translation of each tube. Thus, CTRs are able to steer without the need to exert force on tissue (2, 3). Bending actuation arises due to elastic interaction between the tubes. Since their actuation is based only on the flexing of their own backbones (i.e., the robot's outermost structure) and not on mechanisms such as tendon wires or pneumatic/hydraulic chambers, they are able to steer in hollow regions or liquid-filled cavities. CTRs can also be very thin without sacrificing dexterity.

The first concentric tube–style device was disclosed in a patent application filed in the 1990s (4) and was composed of a straight outer tube and a precurved NiTi wire. The device was proposed for the localization of lesions within the body and, in particular, of nonpalpable lesions within the breast. A volume edited by Cuschieri et al. (5) highlighted for the first time the new directions that concentric tube devices, made of precurved tubular NiTi components, could open up in endoscopic surgeries. A few years later, the German company Daum filed a patent application for a deflectable needle assembly that included a telescoping cannula, a catheter, and a

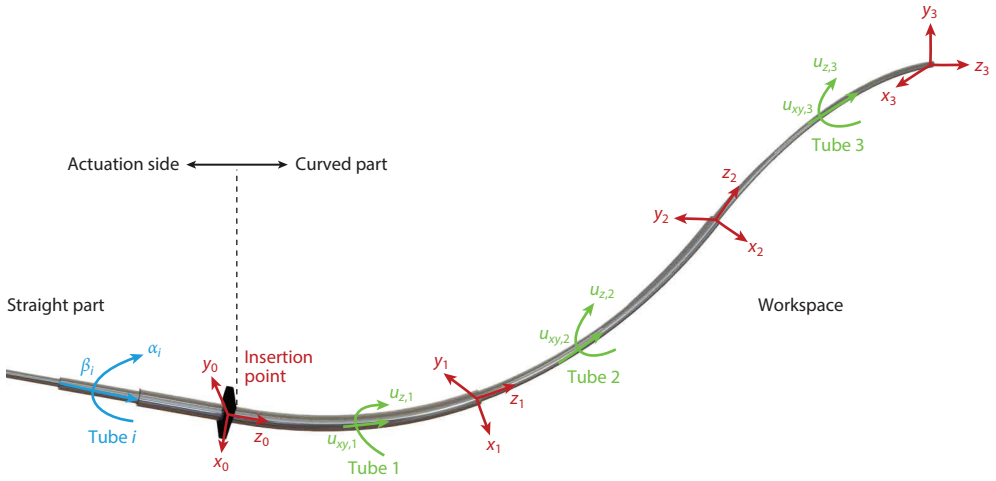

Figure 1

A representative CTR manipulator composed of three precurved NiTi tubes. Each tube can be independently rotated and translated. Tubes are grasped at their respective proximal ends. The actuation variables $\alpha_i(t)$ and $\beta_i(t)$ denote the rotation and translation of the ith tube, respectively, and the variables $u_{z,i}$ and $u_{xy,i}$ denote the torsion and bending of each tube, respectively. Abbreviations: CTR, concentric tube robot; NiTi, nitinol.

stylet (6). The catheter, made from NiTi, was curved at its distal end and axially rotatable within the lumen of the cannula. The first motorized concentric tube system was presented in 2005 by Furusho et al. (7), and the first mechanics-based models were introduced in 2006 by Webster et al. (8) and Sears & Dupont (9). Since then, energy minimization methods, Bernoulli–Euler beam theory, Cosserat rod theory, and, recently, data-driven learning of the forward and inverse kinematics of CTRs have all been explored as modeling approaches for effective robot control. Similar progress has been achieved in the computational design of CTRs, incorporating task considerations and patient-anatomy constraints. Eccentric arrangements of tubes are also being investigated, and multiarm CTRs with straight or flexible backbones have appeared. The former are already being considered for first-in-human evaluation and clinical translation (10). Startups leveraging this technology, such as Virtuoso Surgical (**https://virtuososurgical.net**) and EndoTheia (**https://endotheia.com**), have started working on bringing systems into the operating room.

This review provides an extended literature survey of the aforementioned advancements in the field of CTRs and discusses future opportunities to address current research constraints. We critically discuss the robot prototypes that have been developed along with their design principles, identify theoretical contributions, and compare theoretical models with control theories.

We searched the scientific literature by considering the flagship robotics conferences (e.g., the International Conference on Robotics and Automation, the International Conference on Intelligent Robots and Systems, the International Conference on Biomedical Robotics and Biomechatronics, and Robotics: Science and Systems) and journals (e.g., the *International Journal of Robotics Research*, *Transactions on Robotics*, *IEEE/ASME Transactions on Mechatronics*, *IEEE Transactions on Biomedical Engineering*, *Frontiers in Robotics and AI*, and the *Annual Review of Control, Robotics, and Autonomous Systems*) as well as previous review works (11–13). We exhaustively went through the papers from each conference and journal back to the year that the first paper related to CTRs, or the first issue of a journal, was published. At that stage, we performed the first search using the keywords continuum robot, active cannula, CTR, and soft robot. We then evaluated the papers that had been identified with regard to their forward citations and backward references, read all the papers, and assigned them to one or more categories based on their focus; the main categories of keywords were application and design, analysis and modeling theory, experimental evaluation, and control, which are all echoed in the organization of this article. **Figure 2** shows the number of occurrences of each category per year. In the first few years, the number of publications increases slowly, probably due to the limited number of research groups working on CTRs; subsequently, a steady increase shows the spread of this research. The figure also shows a progressive increase in the number of publications on control of CTRs.

2. MODELING AND CONTROL

A CTR's workspace is determined by the robot tubes' precurvature, stiffness, and length. The joint-to-task-space mapping for a CTR is complex, consisting of unstable equilibrium points that cause snapping (structural instability that causes the robot to rapidly transition from one configuration—i.e., equilibrium state—to another of lesser energy) and concentric constraints resulting in the noncommutativity of the robot input sequence (14, 15). These characteristics complicate the modeling, motion planning, and control of CTRs.

2.1. Modeling

Extensive research on CTR modeling has led to excellent descriptors of CTR shapes for a given set of joint configurations, particularly in the absence of external forces and torques.

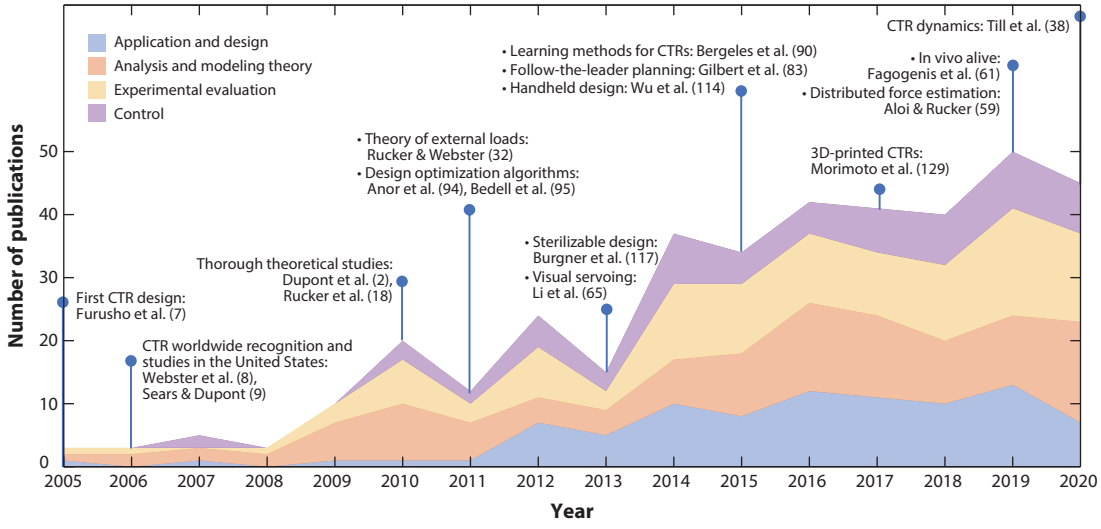

Figure 2

Number of occurrences per year of the four identified categories. Selected works in the research field of CTRs are also shown. Abbreviation: CTR, concentric tube robot.

2.1.1. Quasi-static models. Two of the most widely studied and referenced CTR mechanics models are based on (*a*) weighted curvature superposition (2, 16, 17) and (*b*) differential (variable) curvature kinematics (18). Beam mechanics or Cosserat rod theory and Hooke's material law are utilized as the system conservational (system) and constitutional (material) laws (mechanics) for both of the aforementioned kinematic representations.

In weighted curvature superposition, the system kinematics (the tubes' local shape and orientation) is based on weighted curvature superposition combined with torsional rigidity. The curvature weights are the tubes' bending and torsional structural stiffness values, which form a simple-to-integrate initial value problem that is well suited for providing good real-time numerical performance.

In differential curvature kinematics, the system kinematics is derived via a set of differential equations for curvatures and torsion that is known in continuum robotics as the variable-curvature kinematics. The system kinematics is usually combined with Cosserat rod theory to derive the system's governing equations (18). As a result, a boundary value problem is formed with unknown boundary conditions at the base and tip of the robot backbone, which can be solved via a numerical optimization method, such as single shooting (18). This method is favorable because of its accuracy, generality, and robustness.

Other investigated models include approximating the robot forward map via curve (e.g., truncated Fourier series) fitting (19), forming a lookup table for the robot input–output relation based on precollecting experimental data or precomputing simulation data, simplifying the system's boundary value problem using tube-base force sensing (20), finite shell element modeling based on a piecewise constant strain assumption (21, 22), reduced-order techniques based on curvature (23) and shape polynomial (24) approximation, and learning-based methods (25–27). The effects of external loads have been extensively studied based on the Cosserat rod model (28, 29). A summary of the technical aspects, implementation procedures, advantages, and shortcomings of these methods is presented in **Table 1**, where l is length, ϕ is twist angle, κ is curvature, C is the fitting curve coefficient, $\mathcal{P}$ is the Cartesian position vector, n_t is the number of tubes, n_s is the number of

Table 1 Forward and inverse modeling techniques for concentric tube robots

Model	Reference(s)	States [number]	Inverse kinematics	Dynamic	Inverse kinematics algorithm	Error	Advantages	Disadvantages	Software reference
Curvature superposition (piecewise constant curves)	9, 30	$l_i, \phi_i, \kappa_i, i = 1 \ldots n_s$ $[3n_s]$	Inverse Jacobian, numerical optimization, or lookup table	NA	1. Desired tip position $\mathcal{P}_t$ 2. Piecewise constant curvature fitting 3. Inputs (l_i, ϕ_i) via inverse constant curvature map 4. Mapping for external loads	4 and 1.9 mm (0.3% and 1.3%) without and with load, respectively	Real time Inverse kinematics map Simplest model Multiple solutions	External load only via separate mapping High relative stiffness Only circular constant precurves	37
Differential curvature (truncated Fourier series)	18, 31, 32	$l_i, \kappa_{(s)}, \phi_{i_{(s)}}$, $i = 1 \ldots n_t$ $[\infty]$	Inverse Jacobian, numerical optimization, or lookup table	See Reference 38	1. Form optimization problem based on forward map 2. Boundary conditions initial guess for curvatures 3. Inverse kinematics via numerical optimization	2–12.5 mm (1.5–3.9%)	Inverse kinematics and compliance maps Exact formulation Multiple solutions	Numerically inefficient Initial guess issues Several convergence issues Hard-to-find multiple solutions Limitations on data set richness	38
Approximate forward map	19	$C_i, i = 1 \ldots n_\psi$ $[n_\psi]$	Analytical	No	1. Forward kinematics precomputation 2. Fourier series fitting 3. Inverse kinematics via the fitted mapping	0.03–4.2 mm (0.01–3.1%), 0.06–8.6°	Real time Inverse kinematics and compliance maps Real-time adaptive implementation	Preknown external loading Fixed lengths Fitting convergence issues No multiple solutions	NA
Precomputed lookup table	33	$l_i, \phi_i, \mathcal{P}_t$, $i = 1 \ldots n_s$ $[2n_t + 6]$	Lookup table	No	1. Forward kinematics precomputation 2. Forming lookup table 3. Inverse kinematics via table search	3–21 mm (1–7.5%)	Fast inverse map Inverse kinematics and compliance maps	No external loads No multiple solutions Storage memory issues	39
Forward integration by sensing base loads	34, 35	$l_i, \kappa_{(s)}, \phi_{i_{(s)}}$, $i = 1 \ldots n_t$ $[\infty]$	Multilayer	No	1. Cosserat rod formulation 2. Forward integration with known boundary conditions at $s = 0$	1.5–4.7 mm (1–3%)	Real time Force observation Force compensation controller	Sensitivity to force sensor errors Requires known loading positions Complex setup design No inverse kinematics or compliance map	NA
Discretization (finite shell or constant strain elements)	21, 22, 36	$l_i, \kappa_{ij}, \phi_{ij}, i = 1 \ldots n_t, j = 1 \ldots n_e$ $[3n_t n_e]$	Inverse Jacobian	No	1. Discretized rod formulation 2. Forming an optimization problem 3. Solve for system states	3.3 mm (1.3%) with no load, 2.5–4% with point or distributed load	Possible real-time implementation External loads Finite number of states Multiple solutions	Requires convergence guarantee Computationally expensive Complex inverse kinematics formulation	NA
Reduced-order kinematics (polynomial curve or shape approximation)	23, 24	$C_{ijk}, i = 1 \ldots n_t, j =$ 3 or 4, $k = 0 \ldots n_p$ $[(3 \text{ or } 4) \times n_t \times n_p]$	Inverse Jacobian or optimization	Yes	1. General form shape function 2. Substituting in governing equations (derive linear form) 3. Solve for C_{ijk}	2.5 mm (1.3%)	Possible real-time implementation Inverse kinematics and compliance maps Finite number of states Multiple solutions External loads	Complex derivation Estimation causes error Convergence guarantee needed	24 (TMTDyn)
Deep learning and neural network models	25, 27	Neural network parameters [number of neural network parameters]	Neural network	No	1. Large experimental data set 2. Neural network training 3. Inverse kinematics via the trained neural network	1.36–2.3 mm (0.6–1%), 1.1° (forward); 4 mm (1.7%), 8.3° (inverse)	Fast inverse map Inverse kinematics map High accuracy	Known loading condition No multiple solutions Limitations on data set richess	NA

Abbreviation: NA, not applicable.

overlapping segments, n_e is the number of finite elements, n_ψ is the number of shape functions in a fitting method, n_p is the polynomial order, and i, j, and k are general numerators.

Absolute (Euclidean distance of simulation predictions and robot tip position in experiments) and relative (absolute error value divided by the robot backbone curve length expressed as a percentage) error values are used for experimental verification of theoretical studies. The state-of-the-art normalized error with respect to arc length for the modeling tasks is approximately 1.5–2% (1.5–4.7 mm) (28, 40). The modeling and tracking error can reach values as small as 0.02 mm for carefully optimized tube parameters and simple trajectories (41). Adaptive frameworks, such as truncated Fourier series shape estimation (error of 3 mm, 1.2%) (42) and Kalman filter–based model parameter estimation (2 mm, 0.8%) (43), can improve the accuracy of the physics-based models. Medical applications of CTRs usually call for a positioning accuracy of 1–2 mm (42), implying that models can perform on par with the clinical requirements. It must be noted, however, that most models and controllers perform best in unloaded conditions.

2.1.2. Elastic stability and snapping motion. The relative rotation of the tubes results in the accumulation of torsional energy up to an unstable point where this torsional energy overcomes the bending energy. At such an unstable point, the system's torsional energy is released, causing a rapid movement of the tubes known as snapping. Such sudden high-energy motion is usually undesirable in medical interventions and should be avoided by structural design, motion control, or planning (44). Mathematically, this instability is associated with a bifurcation point in the tube tip twist angle when plotted versus the base input rotation angle. This is equivalent to the appearance of two stable attractors (minima) in the deformation energy plot versus the tubes' base rotation angle (17). The system static formulation has multiple solutions (equilibrium points) at this instance, known as a system with cardinality greater than 1 (45).

The system's linearized governing equations can be used to analyze its local (arbitrary tube number) and global (two-tube systems) stability (45, 46). Alternatively, one can use the relation between the tubes' distal and proximal rotation angles (47), the momentum-free condition at the distal tube ends (48, 49), bifurcation and elastic stability theory (46, 50), or optimal control theories based on the second time derivative of the elastic energy function (51). More recently, the local stability of CTRs with general precurved shapes (e.g., helical) has been investigated as well (45).

Snapping's sudden energy release can also be utilized to perform high-energy tasks, such as driving a suturing needle through a tissue. Such efforts significantly benefit from dynamic models that are able to capture the transient dynamics of snapping (24, 38, 52).

2.1.3. Hysteresis due to tube friction and clearance. CTRs' shapes depend not only on the actuation input values but also on their time history due to the tubes' friction and clearance. These are the main sources of hysteresis in the system. An early investigation by Lock & Dupont (53) that used simple mechanical models suggested that the dominant effect of the frictional force is associated with a concentrated bending moment at the tube ends. More recently, Ha et al. (54) reported that the hysteresis due to distributed torsional friction (as opposed to the tube clearances) is the main source of CTR modeling inaccuracy.

2.1.4. Dynamic modeling. Existing quasi-static models evaluated independently or as part of inverse kinematics approaches cannot capture the system transient dynamics, such as vibration and overshoot due to snapping or high-bandwidth maneuvers when the system inertial forces matter [e.g., for a hyperelastic structure robot (55)] or due to sudden exertion or release of external loads (38). Furthermore, extra modeling layers are needed to capture system hysteresis and Coulomb friction (53). Till et al. (38) presented the first dynamical model for CTRs by extending their

real-time solver for dynamical modeling of continuum robots based on differential curvature kinematics and Cosserat rod mechanics (28, 40). Their model could capture a CTR's transient vibrations after snapping and environmental contact release. However, the employed Cosserat rod–based methods require an infinite number of states and are not suitable for nonlinear control and observation design. Recently, approaches based on modeling with a reduced number of states have attempted to address these challenges (23, 24).

2.2. State Estimation and Observation

State estimation and state observation of a CTR are prerequisites for their control and are discussed next.

2.2.1. Shape estimation. Effective control usually requires real-time shape information about the robot's complex mechanics, especially when external loads are present. Curve-fitting techniques—for example, via Bezier curves (tip error of 1.38 mm, 1.1%) (56) or truncated Fourier series (3 mm, 1.2%) (42), or using trigonometric or data-driven learning of the basis function (3.7 mm) (57)—are employed to observe the robot's overall shape based on visual (58) or limited sensor data.

2.2.2. Force observation. Safe intervention is not possible without force observation and controlled force measurements. Tube deflections are used to formulate an inverse mechanical problem based on Cosserat rod (59) or cantilever beam (60) models to estimate the tubes' distal forces in real time via numerical optimization or an inverse Jacobian formulation, respectively. Fagogenis et al. (61) used sensor fusion based on recordings from a tip camera and a base-fixed force sensor, and Donat et al. (62) employed deep direct cascade learning frameworks and showcased a 2.1% tip force magnitude estimation error.

Distributed force estimation is closer to a clinical scenario. Aloi & Rucker (59) modeled the point and distributed loads based on fitting Fourier series curves and Dirac delta functions, respectively, to comply with the observed backbone shape while satisfying the system mechanics. They reported 6.7% force magnitude and 2% force location error values with a near-zero overall shape estimation error.

2.3. Control

CTR control is the first highlighted task of the robot and the first step to their autonomous deployment and/or telemanipulation.

2.3.1. Visual servoing. Model-free visual servoing techniques (known as eye-in-hand methods) based on recordings from a robot tip camera are the direct solutions for control of CTRs (63–66). In a notable example that included in vivo deployment, Fagogenis et al. (61) utilized this method for autonomous blood vessel navigation by following the arterial wall.

2.3.2. Sampling-based optimization and precomputed lookup tables. Sampling-based path-planning methods via numerical optimization have been widely investigated (31, 67, 68). Obstacle avoidance, global goal convergence, avoidance of unstable configurations, and spatial and temporal stability can be guaranteed by introducing required constraints in well-defined optimization problems alongside standard planning methods, such as rapidly exploring random trees (RRT) (47, 69, 70) and graph search (71). Alternatively, active constraints have been employed for

trajectory tracking, where a sliding-mode-like controller brings the robot tip toward a safe desired trajectory, away from obstacles and unstable configurations (39).

2.3.3. Inverse kinematics and control. **Table 1** presents the different inverse kinematic solutions developed to control a CTR. Unconstrained optimization and inverse Jacobian formulations are the most extensively investigated methods. A notable alternative is an analytical solution when the forward kinematics is approximated by a Fourier series, which is favorable for its simplicity, numerical performance, and accuracy for the trained data set. This, however, comes at the cost of model generality and robustness (19). Alternatively, learning-based controllers have been proposed based on experimental estimation of the system inverse Jacobian (66, 72, 73). Other research has focused on control of multiarm configurations (74, 75) and practical issues with system automation, such as reproducible robot calibration (76).

The tip-tracking accuracies of Jacobian-based and damped least square curve-fitting control methods are approximately 3.2% and 2.5%, respectively. The state-of-the-art multilayer closed-loop control architectures can achieve errors of 0.9% (35) and 0.5% (77). Investigating dexterity (78) and force–velocity manipulability (79) enables real-time planning (in an active constraint and redundant task framework) and control (based on a model predictive closed-loop controller) of a CTR with tip errors as small as 0.3–0.5% (0.5–0.8 mm) (37).

2.3.4. Whole-body and follow-the-leader control. The follow-the-leader method has been the main framework for CTR automation and whole-body control in medical applications (80–82). CTRs cannot perfectly perform follow-the-leader tasks except on paths consisting of a constant curvature or helical curves and a planar arrangement of the tubes with a relatively high stiffness and carefully chosen tube precurvatures and lengths (41, 83). Gilbert et al. (83) proposed a measure for evaluating approximate follow-the-leader performance, showing larger errors for longer tubes and larger differences between the tubes' relative rotation. More recently, Garriga-Casanovas & Rodriguez y Baena (80) showed that helical precurved tubes with an exponentially varying curvature value can be a candidate for follow-the-leader control.

2.3.5. Compliance matrix and stiffness control. With force control in place, calculation and tuning of a robot compliance matrix in the task space can lead to stiffness tuning and impedance control. Jacobian-based methods based on derivative term propagation (32) and multistep mapping (84) have been introduced to calculate and design force controllers based on a CTR tip compliance matrix.

Rucker & Webster (32) presented a calculation framework for Jacobian and compliance matrix calculation along a CTR backbone by considering the necessary partial derivatives in a Cosserat rod–based model. Mahvash & Dupont (84) proposed a two-step transformation map. The CTR's unloaded deformation based on curve superposition was followed by a map for the tube deformation due to external loads based on beam theory. The authors achieved force estimation, stability during environmental contact, and steady-state dynamic performance via the inverse Jacobian method. A formal stability analysis of their proposed controller has not yet been performed. Granna & Burgner (85) extended a similar framework for distal force sensing to a controller for trajectory tracking under external load.

2.4. Planning and Automation

Planning deals with sequential control actions to provide reliable and repeatable safe robot motions regardless of operator experience and fatigue. Stability, goal convergence, task specification

satisfaction (such as impedance control), and obstacle avoidance are the main objectives of a planning paradigm in medical scenarios.

2.4.1. Multiobjective path planning and optimization. Multitask (75, 86) or multilevel (37, 87) planning paradigms are used to satisfy multiple control objectives, such as task-specific planning, trajectory tracking, stability guarantees, self-collision prevention, obstacle avoidance, and even robot structural design optimization.

2.4.2. Whole-shape planning. Whole-shape planning is needed for obstacle avoidance during intraluminal navigation or self-collision avoidance for multiarm CTRs (75). Zhang et al. (88) showed that an RRT-smooth method based on the CTR kinematics can generate path trees that are compliant with whole CTR shapes. Alternatively, precomputing a lookup table of the configuration map is an effective method for selecting collision-free configurations for a desired robot tip position (tip position error of 3 mm, 1%) (39, 89). Integration of further tip correction steps reduces the error to 0.021 mm (0.07%), making this combination the most accurate controller reported in the literature (89).

2.5. Learning-Based Methods: A Surging Paradigm in Research on Concentric Tube Robots

Advancements in neural networks and improved methods for precise data collection have led to the exploration of machine learning as an alternative approach to kinematics modeling. The most common architecture employed is the multilayer perceptron (MLP), which has varying degrees of hidden layers, inputs, and outputs. In the forward kinematics case, the input values can be tube rotations and extensions or actuator inputs directly; the outputs explored are tip 3D position or full tip pose. In inverse kinematics, the inputs and outputs are swapped.

One of the first papers to investigate neural network–based kinematics and inverse kinematics in CTRs was by Bergeles et al. (90). The data set comprised tube rotation/translation and tip pose, generated by the mechanics model implementation from Reference 81. The paper considered an MLP with a single hidden layer for forward kinematics and two hidden layers for inverse kinematics. Either the mean square error at the tip or the robot configuration inputs were used as the loss function that guided training. Data-driven inverse kinematics modeling throughout the full robot workspace was showcased as a challenging problem to overcome in a repeatable way. No experimental evaluation was carried out.

Grassmann et al. (26) also implemented forward and inverse kinematics learning models based on MLP networks with one and two hidden layers, respectively. The data set was generated through a software implementation of the model from Reference 40. The forward kinematics network was able to determine the tip pose with 1% error with respect to the length of the system. The network responsible for the inverse kinematics was trained and evaluated in only a limited region of the workspace and led to 2.8% error. The paper did not include evaluation on a robotic system, however.

Given the challenge in capturing inverse kinematics using MLPs, Iyengar et al. (91) explored deep reinforcement learning. Deep reinforcement learning incorporates agents that dynamically learn by adjusting their actions to maximize a reward function, without requiring a full training data set to be available a priori. Iyengar et al. (91) reported an error of 0.33 mm while following a circle pattern. Solberg (92) evaluated the effects of different agents, and newer work has considered the effects of curricula in deep reinforcement learning for CTRs. As with the works mentioned above, deep reinforcement learning in CTRs has still not been experimentally evaluated.

Notably, Kuntz et al. (27) have carried out an experimental evaluation. They trained an MLP with reduced receptive fields on segmentations of CTR shapes that were approximated using a polynomial basis function. The MLP predicted the coefficients of the basis function, leading to full shape reconstruction. A grid search in hyperparameter space was performed to fine-tune the MLP. The authors also reported improvement in error when using a combination of recorded and simulated data sets over purely simulated data sets. They concluded that pretraining with simulated data followed by retraining with experimental data leads to the best performance.

Other research has considered the most appropriate presentation of network inputs to train forward kinematics networks. Grassmann et al. (26) thoroughly investigated this topic in direct relation to CTRs. Grassmann & Burgner-Kahrs (93) also investigated the effect of input data normalization. Using simulated data led to significant performance improvements, whereas using experimental data did not, possibly because the former had five times as many data points (500,000 versus 100,000).

Recent work has also explored learning of force application. Donat et al. (62) compared the use of an MLP, extreme learning machine, and deep direct cascade learning to estimate contact forces. Deep direct cascade learning was the most effective, with a 3.8% error under a maximal force of 2.29 N.

2.6. Limitations and Future Directions

Available modeling and control methods can achieve tip-positioning errors as small as 0.3 mm (0.5%) (37). It is hard, however, to compare the reported error values in the literature given the differences in the stability of the experimental systems, the limited information provided regarding the workspace coverage, and the differences in the complexity of the test cases. Introducing metrics for comparing different setups' stability and workspace coverage and complexity help to justify reported achievements in the literature.

Despite many recent advances in modeling complementary phenomena, such as hysteresis (54), stability (45), and manipulability (79), there is no unified framework that captures all the necessary elements of modeling and control of a CTR—such as dynamics, hysteresis effects, snapping, compliance analysis, force, position, and shape control—in a numerically efficient way. In a similar vein, no method for combined learning of force estimation and shape estimation exists, and how networks trained on a specific CTR can extrapolate to other CTRs, even if the same number of tubes is present, remains an open research problem. Perhaps generalization beyond the observed data and incorporation of the nonlinear mechanics effects can be addressed by integrating data-driven approaches with physics-based methods to achieve robustness to disturbances that are not present in the data.

3. STRUCTURAL DESIGN AND OPTIMIZATION

Specific surgical tasks and the anatomical environment impose constraints on the design of a CTR. Design methodologies and optimization frameworks have been developed to tailor the workspace, dexterity, and task specificity of CTRs prior to an intervention. Computational design methods aim to maximize performance metrics such as manipulability, stiffness, and stability by fine-tuning characteristics such as tube diameters, lengths, and curvatures through constrained optimization. Constraints may include the requirement to avoid contact with the anatomy, limit the approach angle of the robot to vessels, or push for a reduced overall length and curvature. **Table 2** summarizes the state of the art of computational CTR design methods.

Table 2 Computational designs for concentric tube robots

Reference	Method	Objective function	Optimization variables
94	Global pattern search optimization	1. Min(L and κ) 2. Reach multiple targets 3. Obstacle avoidance	L and κ
95	Global pattern search	1. Min(L and κ) 2. Obstacle avoidance 3. Reach all targets	L and κ
96	Unconstrained nonlinear simplex search	Min(unreachable points)	L and κ
97	RRT	1. Reach multiple targets 2. Obstacle avoidance	L and κ
98	Nelder–Mead simplex algorithm	Max(workspace coverage)	L and κ
49	Study of monotony	Max(stability)	Precurvature function
99	Adaptive simulated annealing and RRT	Max(workspace)	L and κ
81	Nelder–Mead downhill simplex	1. Anatomical constraints 2. Stability 3. Workspace	Number of tubes Bending stiffness and κ
100	Pareto grid search	Reachability and elastic stability	L and κ
101	Fminsearch	Max(workspace coverage)	None
102	Brute-force and greedy algorithms	Max(workspace coverage)	Number and type of aspiration tube
103	Steepest descent	Max(stability)	Combined precurvature
74	Particle swarm optimization	Max(collaborative configurations)	L and κ
86	Multiobjective particle swarm optimization	1. Max(tumor's coverage) 2. Min(ablation overlap)	Ablation objects L and κ
104	Mesh adaptive direct search	1. Min(number of tubes) 2. Max(distance from organs) 3. Follow trajectory	Number of tubes and κ

Abbreviation: RRT, rapidly exploring random trees.

3.1. Design Optimization

Early research was presented by Anor et al. (94) and Bedell et al. (95). Anor et al. (94) used a systematic approach to optimize the design of CTRs for neurosurgical procedures, with a focus on endoscopic choroid plexus ablation. This method for the first time identified the need for either fixed-curvature or variable-curvature sections, while Bedell et al. (95) presented the notion of robot navigation and manipulation sections. In both works, global pattern search optimization determined the length and curvature of each tube in order to reach multiple targets while avoiding contact with brain ventricles and the heart wall and minimizing the tubes' length and curvature.

Burgner et al. (96) presented the use of an unconstrained nonlinear simplex search method in a skull base surgery scenario to minimize unreachable points, introducing the concept of volume coverage in robot design instead of specific point reachability. A torsionally rigid robot kinematic model was considered, and an optimal cannula tube design was acquired when the end effector's tip was within the desired working volume. Burgner et al. (98) provided an in-depth discussion of the idea of volume-based design, advancing their previous work by using a mechanics-based model that included torsional compliance and incorporated workspace constraints related to the robot's entry path in approaching the surgical site. Moreover, they also introduced a new volume-based optimization metric that penalized voids in the robot's workspace. In a similar vein, Granna et al. (102) added the number of tubes, apart from the tubes' curvature, to the design process. The

authors employed a brute-force and greedy algorithm to maximize workspace coverage for intracerebral hemorrhage evacuation. In a later paper, Granna et al. (86) presented a generalization of the previous works; the authors proposed a novel computer-assisted design process that decomposed the problem into task- and robot-specific design optimizations. The method was based on a multiobjective particle swarm optimization algorithm with variable length. The authors used the scenario of laser-induced thermotherapy in the brain to validate their method. The robot-specific design process determined the tube curvature and length of the CTR end effector as well as different configurations. The proposed algorithm was evaluated on real patient data sets.

Drawing inspiration from path planning, Torres et al. (97) employed RRT to acquire CTR designs and reach multiple sites within the bronchial tubes while avoiding the anatomy. The method included for the first time the notion of design coherence, which is based on the observation that the collision-free configuration spaces of robots of similar design are also similar. This was the first work to incorporate mechanics models with torsional compliance.

Bergeles et al. (81) introduced the elastic stability of CTRs in the design optimization by including heuristics that maximize robot stability. Moreover, the effect of section type (variable or fixed curvature) on the boundaries of the workspace was discussed in detail and affected the design methodology and optimization method. The authors used the Nelder–Mead downhill simplex as an optimization algorithm and explored scenarios of hydrocephalus treatment and beating-heart surgery in simulation.

Yang et al. (104) used the number of tubes as an additional optimization variable, along with the tubes' curvature. They introduced geometry-based kinematics in CTR design, which significantly reduced the computational time. The geometry-based method estimated continuous circular curves, while intermediate nodes derived from the desired trajectory determined the number and type of subsections that the final design of the CTR comprised.

It should be noted that all the works mentioned above on CTR design are based on optimization variables and functions that the designer has decided to implement in their method with little or no surgeon input on the final design. In some works (e.g., 47, 86, 94), a surgeon can select the initial entry point or vector and constraints for the initial configuration, but their vast knowledge of patient anatomy and procedure is not fully leveraged. Morimoto et al. (105) created an interface for surgeons to design CTRs for specific patients and procedures, enabling the surgeon to provide more input on the design. The intuitive interface allowed the user to see the anatomical model of interest in 3D and initialize a CTR design by setting a number of via points. The user could alter individual tube parameters until the desired configuration was obtained. Moreover, the interface allowed the user to explore the environment and simulate the CTR's movement through the body.

Design algorithms are not the only way to acquire optimal CTR designs. To minimize the effect of instability, methods for anisotropic patterning of tubes have been studied. Several works and experimental results have shown the promising employment of patterned tubes to achieve higher curvatures while eliminating the problem of snapping. Azimian et al. (106) explored the use of a cellular tube to minimize the bending-to-stiffness ratio. Simulations using finite element analysis derived the optimal design of the cell geometry via trial and error. Experiments using the derived optimal design showed that a patterned tube can exhibit a smooth rotation without snap-through motion. Lee et al. (107) improved on previous work by building a lumped analytical model, examining it with finite element analysis, and providing an in-depth discussion of the patterning of NiTi tubes. The developed experimental system showed that the tubes' patterning can eliminate snapping and decrease the bending-to-stiffness ratio. Similarly, Kim et al. (108) studied the creation of a nonuniform pattern on coaxial tubes to enhance the stiffness of a CTR via a continuously

variable stiffness mechanism. The stiffness change was validated via analytical modeling, finite element method simulation studies, and experimental results, all of which showed an increase in stiffness. Finally, Ai Xin Jue Luo et al. (109) were the first to employ topology optimization methods to acquire the optimal design of patterning so as to decrease the bending-to-stiffness ratio and resolve the snapping problem. They validated the developed method through finite element analysis as well as experimental testing.

3.2. Remarks and Limitations

Methods for computing optimal CTR designs to reach specified positions have been derived by employing different optimization algorithms and taking into account different design variables. Topology optimization methods and finite element analysis have also been used to derive optimal designs with enhanced stability and stiffness. However, a unified framework that takes into account all possible design variables and requirements has not yet been released or deployed in a real-world scenario.

Moreover, new design variables can be included in future optimization methods. Design variables can include metrics used in control [e.g., force or velocity manipulability (110)] or characteristics that describe cooperation in the case of multiarm systems [e.g., triangulation (74)]. These metrics can also be employed as a unified comparison metric even though the community unofficially uses the error per unit length to compare specific work with the state of the art. The stiffness and anisotropy of end effectors are possible candidates for future design optimization algorithms, as there are limitations on the diameters of tubes that can be manufactured. In addition, tissue properties should be taken thoroughly into consideration. Finally, a general analytical model for optimal patterning designs has yet to be derived.

4. CONCENTRIC TUBE ROBOTS IN MEDICAL INTERVENTIONS

In this section, CTR prototypes are organized according to their surgical application. The prototypes discussed have been evaluated on realistic phantoms and/or cadavers or show innovative design characteristics. **Figure 3** provides a pictorial overview of some of the evaluated systems.

4.1. Concentric Tube Robots in Medical Intervention and Surgery

CTRs were originally introduced as slender, flexible robots for challenging surgical interventions and have already been proposed for use in a wealth of medical interventions.

4.1.1. Brain and skull base surgery. Skull base surgery takes place near locations where neurovascular structures enter and exit the brain. It is prescribed for a wide variety of neurological disorders, such as intracerebral hemorrhage, brain tumors, and epilepsy. Rigid instruments limit the effectiveness of procedures because they must follow straight trajectories, which increases the chances of harming critical tissue and structures. When regions deep inside the brain must be reached, conventional approaches can result in heavy trauma to healthy brain tissues. CTRs promise to dexterously access regions within the brain and skull base and deliver therapies to deep-seated pathologies.

Burgner et al. (117) introduced a sterilizable and biocompatible robot with three degrees of freedom (DOFs) for intracerebral hemorrhage evacuation (shown in **Figure 3*g***). The prototype was the first reusable, sterilizable, and operating room–ready actuation unit for CTRs. All of its

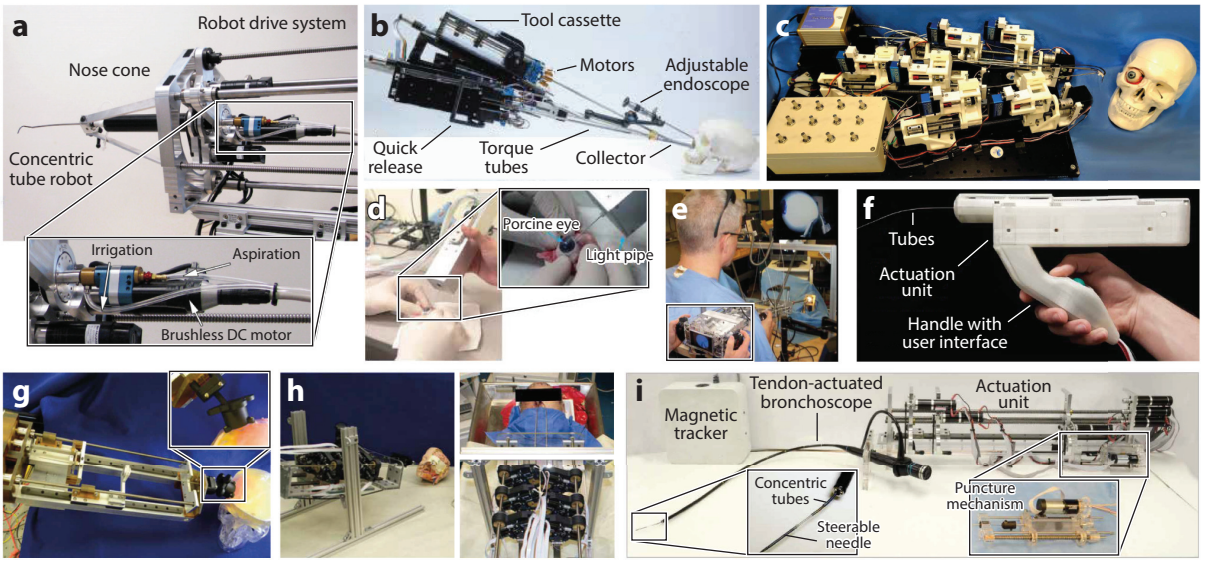

Figure 3

CTRs for various medical applications: (*a*) intracardiac surgery, (*b*) endonasal surgery, (*c*) deep orbital interventions, (*d*) a light pipe for intraocular procedures, (*e*) prostate surgery. (*f*) a handheld CTR for minimally invasive surgery, (*g*) intracerebral hemorrhage evacuation, (*h*) endonasal tumor removal, and (*i*) lung interventions. Abbreviation: CTR, concentric tube robot. Panels *a–i* adapted with permission from References 111–119, respectively.

components were autoclavable and biocompatible, and the motors could be bagged to ensure the sterility of the system. The robot comprised two tubes, with the outer one being straight and the inner one having a curved distal end. The inner aspiration tube was interchangeable during use. The motors could be attached or detached from the transmission through Oldham couplings. Lead screws were used for the translation of the tubes, and the rotation of the inner aspiration tube was achieved via a square shaft that interfaced with a gear train. The authors validated the concept by performing experiments using a gelatin phantom. The phantom was placed in an acrylic box and was made from 10%-by-weight Knox gelatin, while clots were made from Jell-O gelatin.

Burgner et al. (118) developed a telerobotic system for endonasal skull base surgery. The system comprised two concentric tube arms that were made from NiTi and held a ring curette and a gripper (see **Figure 3*b***). A straight manually operated endoscope was used for visualization. The robotic system also comprised two six-DOF input devices and an electromagnetic tracking system. The translation of the tubes was based on the use of a worm gear, which rotates a nut that rides on a stationary lead screw. The worm gear driving the rotation rotated a spring collet, which grasped the base of its respective tube. The robot and the clinical concept were evaluated by performing a mockup surgery on a human cadaver head. The two manipulators entered the nasal passage of the cadaver through a single nostril to show that they could successfully reach the pituitary gland. An updated system (see **Figure 3*a***) included three arms to satisfy real-world surgical workflow requirements (see 112). Each arm was a single interchangeable tube cassette, which was mounted on any of the four module carriers of a base and was locked by a large handle. Motors were placed outside of the module carriers to reinforce sterility. Tube translation was achieved via lead screws, while spur gears and square shafts were used for the rotation. The tool module was made of

autoclavable and biocompatible materials. Visualization was achieved by a Karl Storz Endo-CAMeleon rod lens endoscope with adjustable lens direction. Four additional motors located behind each module carrier translated the modules relative to the robot base, enabling full system insertion or retraction.

4.1.2. Eye and deep orbital interventions. CTRs offer compelling new solutions for challenging intraocular and orbit surgeries, which require dexterous maneuvers of submillimeter surgical tools. The forces that relevant tissues can withstand without damage are minuscule, and the constrained workspace introduces further complications.

The first use of CTRs for vitreoretinal surgery was proposed by Wei et al. (120, 121). The authors developed a 16-DOF hybrid robotic system for applications that require fine dexterous manipulation, such as internal limiting membrane pealing and treatment of severe retinal detachments. The intraocular part of the robot was a two-DOF CTR that comprised a precurved NiTi tube that was extended from a straight cannula. The parallel part of the robot provided global precise positioning of the eye and the surgical instrument. Later, Lin et al. (122) and Wu et al. (114) developed one-arm CTRs with four and three DOFs, respectively. The systems were tested on custom-made phantoms, and the robot developed by Wu et al. (114) was also evaluated on porcine eyes. These were the first systems in which the concept of miniaturizing the actuation design was considered. The system of Lin et al. (122) measured just 66 mm × 52 mm × 29.5 mm, with a linear travel range of 30 mm, corresponding to the eye's diameter. The robot comprised two NiTi tubes, with the diameter of the outer one being less that 23 gauge. The inner tube housed a gripper, which comprised steel forceps with a diameter of 300 μm welded with a piece of 27-gauge stainless steel tube.

The prototype of Wu et al. (114) (shown in **Figure 3*e***) was 40 mm × 40 mm × 210 mm. The outer tube was in the 20-gauge range, while the inner tube, with a bending radius of 30 mm, was less than 23 gauge, with an inner diameter sufficient to house a 25-gauge light pipe. Hollow shaft motors eliminated the need for gears or lead screws and avoided backlash. They were controlled by a custom-made joystick and buttons on the top side of the robot. The robot was very light (total weight of 0.496 kg) to enable handheld operation, and was the first robot proposed to be used in this fashion.

Mitros et al. (113) reported a multiarm CTR system (shown in **Figure 3*f***) for deep orbital interventions, with a focus on optic nerve sheath fenestration. The robot consisted of three arms offering a total of 12 DOFs. The CTR arms accessed the eye orbit and the optic nerve by navigating periocularly, following the eye surface, to reach the position where they collaboratively performed the intervention. One arm held a 1.2-mm chip-on-tip camera (Enable, USA), while the others held a gripper and a cannula. Illumination was achieved through optical fibers housed within the camera body. The robotic prototype was tested on a bespoke phantom of the orbit manufactured based on patient data, as well as on porcine eyes. It was the first multiarm system designed for deep orbital interventions and operations on the optic nerve.

A robotic system first presented by Gilbert (112) for pituitary tumor removal was used by Bruns et al. (10) to remove tumors growing behind the eyes in the orbital apex region. The authors integrated a sterile draping concept for nonsterile components and a cartridge-based tool change approach that eased instrument swaps. The robot was evaluated on a silicone eye phantom housed in a portion of a skull 3D-printed in plastic. Two otolaryncologists performed 10 orbital tumor resections in total while minimizing unnecessary fat removal. The phantom of the tumor was made from silicone, and ballistics gel was cast to simulate orbital fat and connective tissues. The authors developed a modular solution for the electrical hardware that comprised multiple units

with microcontrollers rather than a traditional computer, thereby reducing its cost and size. The distribution of the computational load permitted real-time, synchronous, and closed-loop position control of the motors. The surgeon's interface console was a custom-made mobile cart that housed a high-level control computer, two human–machine interfaces (Phantom Omni haptic devices, 3D Systems, USA) and a 42-inch high-definition monitor. This was the first system that consisted of a complete, clinically practical system that permitted intraoperative interchange of concentric tube instruments.

4.1.3. Fetoscopic interventions. Fetoscopic interventions are unique in their requirement to protect the well-being of both the mother and the fetus. Delicate maneuvers under poor visualization conditions are required, occasionally with oblique lines of sight. Dwyer et al. (123) developed a two-DOF CTR with the primary innovation of being coupled to a KUKA LBR iiwa 7 R800 robotic arm constrained by a remote center of motion. The robot was designed for fetoscopic laser photocoagulation, a minimally invasive surgery used to treat twin–twin transfusion syndrome. The robot was evaluated by scanning a human placenta with a miniature camera (a NanEye Stereo camera, Awaiba, Portugal) at the robot's tip. The tubes were actuated by MX-28 Dynamixel servomotors, with the use of square shafts and gears for the rotation and lead screws for the translation. The robot was controlled via VxWorks (Wind River Systems, USA), providing a soft real-time system.

Vandebroek et al. (124) showcased a multiarm CTR for fetal surgery with a focus on spina bifida, one of the most common birth defects. The authors were the first to explore the macro/micro concept during the robot's design. The robot comprised four arms housed within a rigid insertion sheath with an outer diameter of 11 mm. The robot had two mirrored instrument arms, a camera arm (a NanEye camera, Awaiba, Portugal), and one arm for suction and irrigation. Macromotion was achieved based on concentric tube technology, while the micromotion was enabled by a highly bendable segment actuated by a miniaturized fluidic McKibben muscle with an outer diameter of 1.2 mm.

4.1.4. Cardiac surgery. Heart surgery is an acute procedure that usually requires cutting and spreading the sternum to expose the heart, followed by a cardiopulmonary bypass to perform the final intervention in a nonbeating heart. Interventions on a beating heart obviate the need for the bypass but increase the risk of adverse effects and comorbidity. CTRs have reported potentially game-changing benefits in heart surgery.

Gosline et al. (111, 125) used a CTR prototype (shown in **Figure 3*d***) to deliver metal microelectromechanical systems to intracardiac locations though the patient's neck to the right atrium of the heart. This work was the first to propose the use of CTRs as a means to deliver micromanufactured instruments rather than only as active cannulas or dexterous manipulators. Validation by Vasilyev et al. (126) demonstrated robotic percutaneous beating-heart tissue removal through an in vivo atrial septostomy on a Yorkshire swine. Finally, Fagogenis et al. (61) demonstrated autonomous navigation of a CTR inside the heart of a preclinical porcine in vivo model by ensuring low-force contact with the heart tissue and then following tissue walls to reach a goal location.

4.1.5. Lung interventions. CTRs have also been proposed for early detection of lung cancer. While CTRs are compliant robotic systems, they are rigid and cannot safely conform to the human anatomy unless they are patient specific. To mitigate this issue, Swaney et al. (119) developed a three-stage steering system for lung biopsy and therapy delivery (shown in **Figure 3*i***). The system comprised a bronchoscope housing a CTR; the bronchoscope was used to reach the bronchial wall, while the CTR was used to penetrate the wall and carry the tools necessary for a biopsy. The

robot was validated on a phantom consisting of a bronchial tree (made from plastic tubes) that was embedded in a phantom parenchyma (gelatin) and on ex vivo porcine wall tissue.

Amack et al. (127) improved the concept of accessing the peripheral lung by designing a more compact, modular, multistage robot to retrieve biopsies from lesions in the peripheral regions of the lung. The improved version included a quick-connect mechanism, which allowed rapid tool interchange by employing a concept similar to the one used by Burgner et al. (117). Each tool was preconfigured with a spur gear. The robotic system featured two spring-loaded levers, with adjustable sprint tension to minimize backlash, that were able to deflect to accept the spur gear hub. Finally, the new design featured the first precise, systematic homing protocol to acquire a repeatable home position for all DOFs of the robot, achieving a homing precision with a standard deviation of ± 7.3 μm and $\pm 0.09°$.

4.1.6. Prostate surgery. Transurethral laser prostate surgery was studied by Hendrick et al. (128). CTRs were developed to facilitate holmium laser enucleation of the prostate (HoLEP), which is currently a very challenging procedure. The authors demonstrated the use of a robotic system with two concentric tube manipulators housed within a rigid endoscope (as shown in **Figure 3*b***). The handheld system was suspended from a spring-loaded, counterbalanced boom arm. The two manipulators possessed nine DOFs in total, one comprising three precurved tubes (six DOFs) and one including two tubes, with the outer one being straight (three DOFs). One arm facilitated tissue manipulation and retraction, while the other aimed the laser fiber. The linear motion of the tubes was achieved via lead screws that drove tube carriers on ball screws, and rotation was achieved via square shafts, which transmitted torque through a gear train to each tube. The key innovation of the work was that the user teleoperated the concentric tube arms using joysticks mounted on the system itself. The system has been demonstrated in phantom and cadaver experiments using a procedure for benign prostatic hyperplasia.

4.2. Fabrication Techniques

CTRs are made mostly from NiTi due to its superelastic capabilities. NiTi tubes can be precurved using heat treatment either via the employment of a furnace (113) or via an electric technique that uses Joule heating (14).

To shape-set NiTi tubes using an electric furnace, Mitros et al. (113) machined an aluminum template (Al 2219) with grooves of the desired curvature. They found experimentally that the template should be preheated to 520°C for approximately 10 min to ensure uniform heating when the tubes were inserted. Next, they inserted the tubes into the preheated template and inserted the assembly into the oven at a steady-state temperature of 510–514°C for 30 min. They then immediately cooled the template by rapidly quenching it in cold water. Reliable shape setting was observed for curvatures ranging from 14.5 to 285.7 m^{-1} and diameters ranging from 1 to 2.8 mm.

To decrease the manufacturing time and overall cost and achieve higher accuracy in precurvature setting without the presence of relaxation, Gilbert & Webster (14) proposed an electric technique that uses Joule heating. The authors presented a complete system for closed-loop, high-temperature resistance heating of NiTi tubes. They made the template from inexpensive medium-density fiberboard, used an Arduino microcontroller board to regulate the on–off state of the measured resistance of the heated part, and used a metal–oxide–semiconductor field-effect transistor (MOSFET) to control the flow of current, commanded by the microcontroller. The designed system was evaluated by shape setting 10 wires with a target radius of curvature of 63.7 mm. The mean radius of curvature of the resulting wires was 65.1 mm, with a standard deviation of 1.7 mm.

4.3. Motorized Systems for Minimally Invasive Surgery

In the interest of brevity, we do not discuss in detail all the systems developed solely to evaluate theoretical works. However, systems that present a novel design and were not presented above are discussed here.

Girerd & Morimoto (116) designed a handheld CTR (shown in **Figure 3*c***) that can provide the increased accessibility and dexterity of large robotized devices while maintaining the footprint of a traditional handheld tool. The robot comprised three NiTi tubes with roller gears for the simultaneous rotation and translation of the tubes, creating a lightweight and easy-to-assemble system. It was controlled via a symmetric handheld interface that enabled single-hand operation. Morimoto et al. (129) designed the first 3D-printed CTR, which weighed 490 g and had dimensions of 17.5 inches × 3.5 inches × 4 inches. The robot was composed of three tubes and six DOFs in total, and demonstrated experimentally the precision and accuracy that a 3D-printed system can have.

Childs & Rucker (55) presented the first continuum robot based on a pair of concentric precurved bellows. Each bellow rotated axially at its base, allowing independent control of the end effector's curvature and bending plane. The authors developed a 3D-printed system as a proof of concept and performed experiments to demonstrate its payload capacity and validate their theoretical work. This was the first proposal of a continuum robot based on concentric tube technology that could be used as a soft gripper and in general, nonmedical applications.

4.4. Summary of Applied Research on Concentric Tube Robots in Medicine

The design variables that should be considered when designing a CTR are determined by the application that the robot will be used for. They include the diameter of the manipulator, the number of tubes, the material, the curvature, and the stiffness of each tube. The DOFs that the robot should possess, the output force range, and the type of transmission (which affects the friction and the backdrivability of the system) should be taken into account as well.

CTRs can be either stand-alone robotic systems or part of a hybrid system based on the required DOFs and the intended intervention. Most CTRs are stand-alone systems, to take advantage of the miniature end effector and the increased curvature they can possess. The use of hybrid systems (e.g., combining either a parallel robot or a flexible catheter with a CTR) results in systems with no unstable configurations but at the expense of the end effector's dimensions. The overall system, however, ends up being more complex when hardware design is considered.

Several challenges should be addressed prior to the employment of CTRs in clinical settings. Safety during an intervention is one of the most important requirements. The employment of several sensors and the use of the robot by an experimental surgeon can minimize the risk of complications. Moreover, the size and placement of a robot in the operating room should not interfere with the surgical procedure, as the space in an operating room is limited. CTRs can be mounted on either robotic manipulators or passive articulated arms, which can be moved aside when they are not needed. Work on miniaturizing CTRs and surgical tools is underway to minimize their hardware footprint.

The remarks on the design of CTRs based on the prototypes presented above can be summarized by saying that the components should be biocompatible and the tools should be interchangeable. If the ultimate goal is to deploy robots in the operating room, the sterility of the system should be considered. This can be achieved by using biocompatible materials and bagging the motors when they are close to the surgical area. Furthermore, the ability of the system to house a miniature camera at its end effector to visualize the surgical area is critical when visualization through other modalities is not possible. Finally, the research trend is to consider multiarm

systems because of the need to manipulate tissue and deliver more than one tool to the surgical area at the same time.

It should be highlighted that startups leveraging this technology have appeared, showcasing its promise. Virtuoso Surgical and EndoTheia are two startup companies that have come from the Medical Engineering and Discovery Lab at Vanderbilt University, with the aim of bringing CTRs to operating rooms and commercializing steerable sheaths for flexible endoscopy, respectively.

5. CONCLUSION

Over the past few decades, CTRs have matured from a relatively niche area of research to the point where impressive results have been achieved in modeling accuracy, control, system design, and applications. This review has attempted to capture the historical transition from low-fidelity models to the complete incorporation of nonlinear behaviors in system dynamics, the evolution of computational robot design approaches, and the full spectrum of innovative engineered robots. Each section identified relevant research gaps, indicating potential future areas of investigation. Notably, data-driven modeling methods are on the rise, and the systems are taking their first steps toward clinical translation.

DISCLOSURE STATEMENT

The authors are not aware of any affiliations, memberships, funding, or financial holdings that might be perceived as affecting the objectivity of this review.

ACKNOWLEDGMENTS

The authors' research is supported by a European Research Council Starting Grant (714562).

LITERATURE CITED

1. Vitiello V, Lee SL, Cundy TP, Yang GZ. 2013. Emerging robotic platforms for minimally invasive surgery. *IEEE Rev. Biomed. Eng.* 6:111–26
2. Dupont PE, Lock J, Itkowitz B, Butler E. 2010. Design and control of concentric tube robots. *IEEE Trans. Robot.* 26:209–25
3. Webster RJ, Jones BA. 2010. Design and kinematic modeling of constant curvature continuum robots: a review. *Int. J. Robot. Res.* 29:1661–83
4. Bates BL, Hall TA, Osborne TA. 1993. *Guide for localizing a nonpalpable breast lesion*. US Patent 5,221,269
5. Cuschieri A, Buess G, Perissat J, eds. 1992. *Operative Manual of Endoscopic Surgery*. Berlin: Springer
6. Daum WR, Schalgdorf N. 1995. *Deflectable needle assembly*. US Patent 6,572,593
7. Furusho J, Ono T, Murai R, Fujimoto T, Chiba Y, Horio H. 2005. Development of a curved multi-tube (CMT) catheter for percutaneous umbilical blood sampling and control methods of CMT catheters for solid organs. In *2005 IEEE International Conference on Mechatronics and Automation*, Vol. 1, pp. 410–15. Piscataway, NJ: IEEE
8. Webster RJ, Okamura AM, Cowan NJ. 2006. Toward active cannulas: miniature snake-like surgical robots. In *2006 IEEE/RSJ International Conference on Intelligent Robots and Systems*, pp. 2857–63. Piscataway, NJ: IEEE
9. Sears P, Dupont PE. 2006. A steerable needle technology using curved concentric tubes. In *2006 IEEE International Conference on Intelligent Robots and Systems*, pp. 2850–56. Piscataway, NJ: IEEE
10. Bruns TL, Remirez AA, Emerson MA, Lathrop RA, Mahoney AW, et al. 2021. A modular, multi-arm concentric tube robot system with application to transnasal surgery for orbital tumors. *Int. J. Robot. Res.* 40:521–33

11. Gilbert HB, Rucker DC, Webster RJ III. 2016. Concentric tube robots: the state of the art and future directions. In *Robotics Research: The 16th International Symposium ISRR*, ed. M Inaba, P Corke, pp. 253–69. Cham, Switz.: Springer
12. Mahoney AW, Gilbert HB, Webster RJ III. 2018. A review of concentric tube robots: modeling, control, design, planning, and sensing. In *The Encyclopedia of Medical Robotics*, Vol. 1: *Minimally Invasive Surgical Robotics*, ed. R Patel, pp. 181–202. Singapore: World Sci.
13. Alfalahi H, Renda F, Stefanini C. 2020. Concentric tube robots for minimally invasive surgery: current applications and future opportunities. *IEEE Trans. Med. Robot. Bionics* 2:410–24
14. Gilbert HB, Webster RJ III. 2016. Rapid, reliable shape setting of superelastic nitinol for prototyping robots. *IEEE Robot. Autom. Lett.* 1:98–105
15. Alfalahi H, Renda F, Stefanini C. 2020. Concentric tube robots for minimally invasive surgery: current applications and future opportunities. *IEEE Trans. Med. Robot. Bionics* 2:410–24
16. Sears P, Dupont PE. 2007. Inverse kinematics of concentric tube steerable needles. In *2007 IEEE International Conference on Robotics and Automation*, pp. 1887–92. Piscataway, NJ: IEEE
17. Webster RJ, Romano JM, Cowan NJ, Webster RJ III, Romano JM, Cowan NJ. 2009. Mechanics of precurved-tube continuum robots. *IEEE Trans. Robot.* 25:67–78
18. Rucker DC, Jones BA, Webster RJ. 2010. A geometrically exact model for externally loaded concentric tube continuum robots. *IEEE Trans. Robot.* 26:769–80
19. Dupont PE, Lock J, Itkowitz B. 2010. Real-time position control of concentric tube robots. In *2010 IEEE International Conference on Robotics and Automation*, pp. 562–68. Piscataway, NJ: IEEE
20. Xu R, Asadian A, Naidu AS, Patel RV. 2013. Position control of concentric-tube continuum robots using a modified Jacobian-based approach. In *2013 IEEE International Conference on Robotics and Automation*, pp. 5813–18. Piscataway, NJ: IEEE
21. Baek C, Yoon K, Kim DN. 2016. Finite element modeling of concentric-tube continuum robots. *Struct. Eng. Mech.* 57:809–21
22. Pourafzal M, Talebi HA, Rabenorosoa K. 2021. Piecewise constant strain kinematic model of externally loaded concentric. *Mechatronics* 74:102502
23. Renda F, Messer C, Rucker C, Boyer F. 2021. A sliding-rod variable-strain model for concentric tube robots. *IEEE Robot. Autom. Lett.* 6:3451–58
24. Sadati S, Mitros Z, Henry R, Da Cruz L, Bergeles C. 2020. *Reduced-order real-time dynamics of concentric tube robots: a polynomial shape (PS) parametrization*. Tech. Rep., King's College London, London
25. Fagogenis G, Bergeles C, Dupont PE. 2016. Adaptive nonparametric kinematic modeling of concentric tube robots. In *2016 IEEE International Conference on Intelligent Robots and Systems*, pp. 4324–29. Piscataway, NJ: IEEE
26. Grassmann R, Modes V, Burgner-Kahrs J. 2018. Learning the forward and inverse kinematics of a 6-DOF concentric tube continuum robot in SE(3). In *2018 IEEE/RSJ International Conference on Intelligent Robots and Systems*, pp. 5125–32. Piscataway, NJ: IEEE
27. Kuntz A, Sethi A, Webster RJ, Alterovitz R. 2020. Learning the complete shape of concentric tube robots. *IEEE Trans. Med. Robot. Bionics* 2:140–47
28. Rucker DC, Jones BA, Webster RJ. 2010. A model for concentric tube continuum robots under applied wrenches. In *2010 IEEE International Conference on Robotics and Automation*, pp. 1047–52. Piscataway, NJ: IEEE
29. Lock J, Laing G, Mahvash M, Dupont PE. 2010. Quasistatic modeling of concentric tube robots with external loads. In *2010 IEEE/RSJ International Conference on Intelligent Robots and Systems*, pp. 2325–32. Piscataway, NJ: IEEE
30. Webster RJ, Romano JM, Cowan NJ. 2008. Kinematics and calibration of active cannulas. In *2008 IEEE International Conference on Robotics and Automation*, pp. 3888–95. Piscataway, NJ: IEEE
31. Lyons LA, Webster RJ, Alterovitz R. 2009. Motion planning for active cannulas. In *2009 IEEE/RSJ International Conference on Intelligent Robots and Systems*, pp. 801–6. Piscataway, NJ: IEEE
32. Rucker DC, Webster RJ. 2011. Computing Jacobians and compliance matrices for externally loaded continuum robots. In *2011 IEEE International Conference on Robotics and Automation*, pp. 945–50. Piscataway, NJ: IEEE

33. Torres LG, Baykal C, Alterovitz R. 2014. Interactive-rate motion planning for concentric tube robots. In *2014 IEEE International Conference on Robotics and Automation*, pp. 1915–21. Piscataway, NJ: IEEE
34. Xu R, Patel RV. 2012. A fast torsionally compliant kinematic model of concentric tube robots. In *2012 IEEE International Conference of Engineering in Medicine and Biology*, pp. 904–7. Piscataway, NJ: IEEE
35. Xu R, Asadian A, Atashzar SF, Patel RV. 2014. Real-time trajectory tracking for externally loaded concentric-tube robots. In *2014 IEEE International Conference on Robotics and Automation*, pp. 4374–79. Piscataway, NJ: IEEE
36. Ha J, Dupont PE. 2017. Designing stable concentric tube robots using piecewise straight tubes. *IEEE Robot. Autom. Lett.* 2:298–304
37. Khadem M, O'Neill J, Mitros Z, Da Cruz L, Bergeles C. 2020. Autonomous steering of concentric tube robots via nonlinear model predictive control. *IEEE Trans. Robot.* 36:1595–602
38. Till J, Aloi V, Riojas KE, Anderson PL, Webster RJ, Rucker C. 2020. A dynamic model for concentric tube robots. *IEEE Trans. Robot.* 36:1704–18
39. Leibrandt K, Bergeles C, Yang GZ. 2017. Concentric tube robots: rapid, stable path-planning and guidance for surgical use. *IEEE Robot. Autom. Mag.* 24(2):42–53
40. Rucker DC, Webster RJ, Chirikjian GS, Cowan NJ. 2010. Equilibrium conformations of concentric-tube continuum robots. *Int. J. Robot. Res.* 29:1263–80
41. Girerd C, Rabenorosoa K, Rougeot P, Renaud P. 2017. Towards optical biopsy of olfactory cells using concentric tube robots with follow-the-leader deployment. In *2017 IEEE/RSJ International Conference on Intelligent Robots and Systems*, pp. 5661–887. Piscataway, NJ: IEEE
42. Kim C, Ryu SC, Dupont PE. 2015. Real-time adaptive kinematic model estimation of concentric tube robots. In *2015 IEEE/RSJ International Conference on Intelligent Robots and Systems*, pp. 3214–19. Piscataway, NJ: IEEE
43. Jang C, Ha J, Dupont PE, Park FC. 2016. Toward on-line parameter estimation of concentric tube robots using a mechanics-based kinematic model. In *2016 IEEE/RSJ International Conference on Intelligent Robots and Systems*, pp. 2400–5. Piscataway, NJ: IEEE
44. Ha J, Park FC, Dupont PE. 2017. Optimizing tube precurvature to enhance the elastic stability of concentric tube robots. *IEEE Trans. Robot.* 33:22–37
45. Peyron Q, Rabenorosoa K, Andreff N, Renaud P. 2019. A numerical framework for the stability and cardinality analysis of concentric tube robots: introduction and application to the follow-the-leader deployment. *Mech. Mach. Theory* 132:176–92
46. Hendrick RJ, Gilbert HB, Webster RJ. 2015. Designing snap-free concentric tube robots: a local bifurcation approach. In *2015 IEEE International Conference on Robotics and Automation*, pp. 2256–63. Piscataway, NJ: IEEE
47. Bergeles C, Dupont PE. 2013. Planning stable paths for concentric tube robots. In *2013 IEEE/RSJ International Conference on Intelligent Robots and Systems*, pp. 3077–82. Piscataway, NJ: IEEE
48. Xu R, Atashzar SF, Patel RV. 2014. Kinematic instability in concentric tube robots: modeling and analysis. In *2014 IEEE RAS/EMBS International Conference on Biomedical Robotics and Biomechatronics*, pp. 163–68. Piscataway, NJ: IEEE
49. Ha J, Park FC, Dupont PE. 2014. Achieving elastic stability of concentric tube robots through optimization of tube precurvature. In *2014 IEEE/RSJ International Conference on Intelligent Robots and Systems*, pp. 864–70. Piscataway, NJ: IEEE
50. Gilbert HB, Hendrick RJ, Webster RJ III. 2016. Elastic stability of concentric tube robots: a stability measure and design test. *IEEE Trans. Robot.* 32:20–35
51. Ha J, Park FC, Dupont PE. 2016. Elastic stability of concentric tube robots subject to external loads. *IEEE Trans. Biomed. Eng.* 63:1116–28
52. Riojas KE, Hendrick RJ, Webster RJ. 2018. Can elastic instability be beneficial in concentric tube robots? *IEEE Robot. Autom. Lett.* 3:1624–30
53. Lock J, Dupont PE. 2011. Friction modeling in concentric tube robots. In *2011 IEEE International Conference on Robotics and Automation*, pp. 1139–46. Piscataway, NJ: IEEE
54. Ha J, Fagogenis G, Dupont PE. 2019. Modeling tube clearance and bounding the effect of friction in concentric tube robot kinematics. *IEEE Trans. Robot.* 35:353–70

55. Childs JA, Rucker C. 2020. Concentric precurved bellows: new bending actuators for soft robots. *IEEE Robot. Autom. Lett.* 5:1215–22
56. Wang J, Lu Y, Zhang C, Song S, Meng MQ. 2017. Pilot study on shape sensing for continuum tubular robot with multi-magnet tracking algorithm. In *2017 IEEE International Conference on Robotics and Biomimetics*, pp. 1165–70. Piscataway, NJ: IEEE
57. Lobaton EJ, Fu J, Torres LG, Alterovitz R. 2013. Continuous shape estimation of continuum robots using X-ray images. In *2013 IEEE International Conference on Robotics and Automation*, pp. 725–32. Piscataway, NJ: IEEE
58. Vandini A, Bergeles C, Glocker B, Giataganas P, Yang GZ. 2017. Unified tracking and shape estimation for concentric tube robots. *IEEE Trans. Robot.* 33:901–15
59. Aloi VA, Rucker DC. 2019. Estimating loads along elastic rods. In *2019 International Conference on Robotics and Automation*, pp. 2867–73. Piscataway, NJ: IEEE
60. Wei W, Simaan N. 2012. Modeling, force sensing, and control of flexible cannulas for microstent delivery. *J. Dyn. Syst. Meas. Control* 134:041004
61. Fagogenis G, Mencattelli M, Machaidze Z, Rosa B, Price K, et al. 2019. Autonomous robotic intracardiac catheter navigation using haptic vision. *Sci. Robot.* 4:eaaw1977
62. Donat H, Lilge S, Burgner-Kahrs J, Steil JJ. 2020. Estimating tip contact forces for concentric tube continuum robots based on backbone deflection. *IEEE Trans. Med. Robot. Bionics* 2:619–30
63. Wu K, Wu L, Lim CM, Ren H. 2015. Model-free image guidance for intelligent tubular robots with pre-clinical feasibility study: towards minimally invasive trans-orifice surgery. In *2015 IEEE International Conference on Information and Automation*, pp. 749–54. Piscataway, NJ: IEEE
64. Kudryavtsev AV, Chikhaoui MT, Liadov A, Rougeot P, Spindler F, et al. 2018. Eye-in-hand visual servoing of concentric tube robots. *IEEE Robot. Autom. Lett.* 3:2315–21
65. Li X, Choi T, Chun H, Gim S, Lee S, et al. 2013. Active cannula robot with misorientation auto-recovery camera: a method to improve hand-eye coordination in minimally invasive surgery. In *2013 International Conference on Control, Automation and Systems*, pp. 276–80. Piscataway, NJ: IEEE
66. Wu L, Wu K, Ren H. 2016. Towards hybrid control of a flexible curvilinear surgical robot with visual/haptic guidance. In *IEEE/RSJ International Conference on Intelligent Robots and Systems*, pp. 501–7. Piscataway, NJ: IEEE
67. Lyons LA, Webster RJ, Alterovitz R. 2010. Planning active cannula configurations through tubular anatomy. In *2010 IEEE International Conference on Robotics and Automation*, pp. 2082–87. Piscataway, NJ: IEEE
68. Kuntz A, Fu M, Alterovitz R. 2019. Planning high-quality motions for concentric tube robots in point clouds via parallel sampling and optimization. In *2019 IEEE/RSJ International Conference on Intelligent Robots and Systems*, pp. 2205–12. Piscataway, NJ: IEEE
69. Torres LG, Alterovitz R. 2011. Motion planning for concentric tube robots using mechanics-based models. In *2011 IEEE/RSJ International Conference on Intelligent Robots and Systems*, pp. 5153–59. Piscataway, NJ: IEEE
70. Baykal C, Alterovitz R. 2017. Asymptotically optimal design of piecewise cylindrical robots using motion planning. In *Robotics: Science and Systems XIII*, ed. N Amato, S Srinivasa, N Ayanian, S Kuindersma, pap. 20. N.p.: Robot. Sci. Syst. Found.
71. Fu M, Kuntz A, Salzman O, Alterovitz R. 2019. Toward asymptotically-optimal inspection planning via efficient near-optimal graph search. In *Robotics: Science and Systems XV*, ed. A Bicchi, H Kress-Gazit, S Hutchinson, pap. 57. N.p.: Robot. Sci. Syst. Found.
72. Baran Y, Rabenorosoa K, Laurent GJ, Rougeot P, Andreff N, Tamadazte B. 2017. Preliminary results on OCT-based position control of a concentric tube robot. In *2017 IEEE/RSJ International Conference on Intelligent Robots and Systems*, pp. 3000–5. Piscataway, NJ: IEEE
73. Lu Y, Zhang C, Song S, Meng MQ. 2017. Precise motion control of concentric-tube robot based on visual servoing. In *2017 IEEE International Conference on Information and Automation*, pp. 299–304. Piscataway, NJ: IEEE
74. Chikhaoui MT, Granna J, Starke J, Burgner-Kahrs J. 2018. Toward motion coordination control and design optimization for dual-arm concentric tube continuum robots. *IEEE Robot. Autom. Lett.* 3:1793–800

75. Sabetian S, Looi T, Diller ED, Drake J. 2019. Self-collision detection and avoidance for dual-arm concentric tube robots. *IEEE Robot. Autom. Lett.* In press. **https://doi.org/10.1109/LRA.2019.2933194**
76. Modes V, Burgner-Kahrs J. 2020. Calibration of concentric tube continuum robots: automatic alignment of precurved elastic tubes. *IEEE Robot. Autom. Lett.* 5:103–10
77. Wu K, Zhu G, Wu L, Gao W, Song S, et al. 2019. Safety-enhanced model-free visual servoing for continuum tubular robots through singularity avoidance in confined environments. *IEEE Access* 7:21539–58
78. Leibrandt K, Bergeles C, Yang GZ. 2017. Implicit active constraints for concentric tube robots based on analysis of the safe and dexterous workspace. In *2017 IEEE/RSJ International Conference on Intelligent Robots and Systems*, pp. 193–200. Piscataway, NJ: IEEE
79. Khadem M, Da Cruz L, Bergeles C. 2018. Force/velocity manipulability analysis for 3D continuum robots. In *2018 IEEE/RSJ International Conference on Intelligent Robots and Systems*, pp. 4920–26. Piscataway, NJ: IEEE
80. Garriga-Casanovas A, Rodriguez y Baena F. 2018. Complete follow-the-leader kinematics using concentric tube robots. *Int. J. Robot. Res.* 37:197–222
81. Bergeles C, Gosline AH, Vasilyev NV, Codd PJ, del Nido PJ, Dupont PE. 2015. Concentric tube robot design and optimization based on task and anatomical constraints. *IEEE Trans. Robot.* 31:67–84
82. Girerd C, Kudryavtsev AV, Rougeot P, Renaud P, Rabenorosoa K, Tamadazte B. 2020. SLAM-based follow-the-leader deployment of concentric tube robots. *IEEE Robot. Autom. Lett.* 5:548–55
83. Gilbert HB, Neimat J, Webster RJ. 2015. Concentric tube robots as steerable needles: achieving follow-the-leader deployment. *IEEE Trans. Robot.* 31:246–58
84. Mahvash M, Dupont PE. 2011. Stiffness control of surgical continuum manipulators. *IEEE Trans. Robot.* 27:334–45
85. Granna J, Burgner J. 2014. Characterizing the workspace of concentric tube continuum robots. In *ISR/Robotik 2014: 41st International Symposium on Robotics*, pp. 1–7. Piscataway, NJ: IEEE
86. Granna J, Nabavi A, Burgner-Kahrs J. 2019. Computer-assisted planning for a concentric tube robotic system in neurosurgery. *Int. J. Comput. Assist. Radiol. Surg.* 14:335–44
87. Morimoto T, Greer J, Hawkes E, Okamura A, Hsieh M. 2017. Design, fabrication, and testing of patient specific concentric tube robots for nonlinear renal access and mass ablation. *J. Urol.* 197:e817
88. Zhang D, Wang J, Yang X, Song S, Meng MQ. 2018. RRT*-smooth algorithm applied to motion planning of concentric tube robots. In *2018 IEEE International Conference on Information and Automation*, pp. 487–93. Piscataway, NJ: IEEE
89. Torres LG, Kuntz A, Gilbert HB, Swaney PJ, Hendrick RJ, et al. 2015. A motion planning approach to automatic obstacle avoidance during concentric tube robot teleoperation. In *2015 IEEE International Conference on Robotics and Automation*, pp. 2361–67. Piscataway, NJ: IEEE
90. Bergeles C, Lin FY, Yang GZ. 2015. Concentric tube robot kinematics using neural networks. In *The Hamlyn Symposium on Medical Robotics*, ed. GZ Yang, A Darzi, pp. 13–14. London: R. Geogr. Soc./Imp. Coll. Lond.
91. Iyengar K, Dwyer G, Stoyanov D. 2020. Investigating exploration for deep reinforcement learning of concentric tube robot control. *Int. J. Comput. Assist. Radiol. Surg.* 15:1157–65
92. Solberg FS. 2020. *Effect of demonstrations for deep reinforcement learning-based control of concentric tube robots*. MS Thesis, Stanford Univ., Stanford, CA
93. Grassmann R, Burgner-Kahrs J. 2019. On the merits of joint space and orientation representations in learning the forward kinematics in SE(3). In *Robotics: Science and Systems XV*, ed. A Bicchi, H Kress-Gazit, S Hutchinson, pap. 17. N.p.: Robot. Sci. Syst. Found.
94. Anor T, Madsen JR, Dupont P. 2011. Algorithms for design of continuum robots using the concentric tubes approach: a neurosurgical example. In *2011 IEEE International Conference on Robotics and Automation*, pp. 667–73. Piscataway, NJ: IEEE
95. Bedell C, Lock J, Gosline A, Dupont PE. 2011. Design optimization of concentric tube robots based on task and anatomical constraints. In *2011 IEEE International Conference on Robotics and Automation*, pp. 398–403. Piscataway, NJ: IEEE

96. Burgner J, Swaney PJ, Rucker DC, Gilbert HB, Nill ST, et al. 2011. A bimanual teleoperated system for endonasal skull base surgery. In *2011 IEEE/RSJ International Conference on Intelligent Robots and Systems*, pp. 2517–23. Piscataway, NJ: IEEE
97. Torres LG, Webster RJ, Alterovitz R. 2012. Task-oriented design of concentric tube robots using mechanics-based models. In *2012 IEEE/RSJ International Conference on Intelligent Robots and Systems*, pp. 4449–55. Piscataway, NJ: IEEE
98. Burgner J, Gilbert HB, Webster RJ. 2013. On the computational design of concentric tube robots: incorporating volume-based objectives. In *2013 IEEE International Conference on Robotics and Automation*, pp. 1193–98. Piscataway, NJ: IEEE
99. Baykal C. 2015. *Design optimization algorithms for concentric tube robots*. MS Thesis, Univ. N.C., Chapel Hill
100. Boushaki MN. 2016. *Design optimization and control for concentric tube robot in assisted single-access laparoscopic surgery*. PhD Thesis, Univ. Montpellier, Montpellier, Fr.
101. Noh G, Yoon SY, Yoon S, Kim K, Lee W, et al. 2016. Expeditious design optimization of a concentric tube robot with a heat-shrink plastic tube. In *2016 IEEE International Conference on Intelligent Robots and Systems*, pp. 3671–76. Piscataway, NJ: IEEE
102. Granna J, Guo Y, Weaver KD, Burgner-Kahrs J. 2016. Comparison of optimization algorithms for a tubular aspiration robot for maximum coverage in intracerebral hemorrhage evacuation. *J. Med. Robot. Res.* 02:1750004
103. Ha J, Dupont PE. 2017. Incorporating tube-to-tube clearances in the kinematics of concentric tube robots. In *2017 IEEE International Conference on Robotics and Automation*, pp. 6730–36. Piscataway, NJ: IEEE
104. Yang X, Song S, Liu L, Yan T, Meng MQ. 2019. Design and optimization of concentric tube robots based on surgical tasks, anatomical constraints and follow-the-leader deployment. *IEEE Access* 7:173612–25
105. Morimoto TK, Greer JD, Hsieh MH, Okamura AM. 2016. Surgeon design interface for patient-specific concentric tube robots. In *2016 IEEE International Conference on Biomedical Robotics and Biomechatronics*, pp. 41–48. Piscataway, NJ: IEEE
106. Azimian H, Francis P, Looi T, Drake J. 2014. Structurally-redesigned concentric-tube manipulators with improved stability. In *2014 IEEE/RSJ International Conference on Intelligent Robots and Systems*, pp. 2030–35. Piscataway, NJ: IEEE
107. Lee D, Kim J, Kim J, Baek C, Noh G, et al. 2015. Anisotropic patterning to reduce instability of concentric-tube robots. *IEEE Trans. Robot.* 31:1311–23
108. Kim J, Choi WY, Kang S, Kim C, Cho KJ. 2019. Continuously variable stiffness mechanism using nonuniform patterns on coaxial tubes for continuum microsurgical robot. *IEEE Trans. Robot.* 35:1475–87
109. Ai Xin Jue Luo K, Looi T, Sabetian S, Drake J. 2018. Designing concentric tube manipulators for stability using topology optimization. In *2018 IEEE/RSJ International Conference on Intelligent Robots and Systems*, pp. 1764–69. Piscataway, NJ: IEEE
110. Khadem M, O'Neill J, Mitros Z, Da Cruz L, Bergeles C. 2019. Autonomous steering of concentric tube robots for enhanced force/velocity manipulability. In *2019 IEEE International Conference on Intelligent Robots and Systems*, pp. 2197–204. Piscataway, NJ: IEEE
111. Gosline AH, Vasilyev NV, Veeramani A, Wu M, Schmitz G, et al. 2012. Metal MEMS tools for beating-heart tissue removal. In *2012 IEEE International Conference on Robotics and Automation*, pp. 1921–26. Piscataway, NJ: IEEE
112. Gilbert HB. 2016. *Concentric tube robots: design, deployment, and stability*. PhD Thesis, Vanderbilt Univ., Nashville, TN
113. Mitros Z, Sadati S, Seneci C, Bloch E, Leibrandt K, et al. 2020. Optic nerve sheath fenestration with a multi-arm continuum robot. *IEEE Robot. Autom. Lett.* 5:4874–81
114. Wu L, Tan BLW, Ren H. 2015. Prototype development of a hand-held robotic light pipe for intraocular procedures. In *2015 IEEE International Conference on Robotics and Biomimetics*, pp. 368–73. Piscataway, NJ: IEEE
115. Hendrick RJ, Herrell SD, Webster RJ. 2014. A multi-arm hand-held robotic system for transurethral laser prostate surgery. In *2014 IEEE International Conference on Robotics and Automation*, pp. 2850–55. Piscataway, NJ: IEEE

116. Girerd C, Morimoto TK. 2021. Design and control of a hand-held concentric tube robot for minimally invasive surgery. *IEEE Trans. Robot.* 37:1022–38
117. Burgner J, Swaney PJ, Lathrop RA, Weaver KD, Webster RJ. 2013. Debulking from within: a robotic steerable cannula for intracerebral hemorrhage evacuation. *IEEE Trans. Biomed. Eng.* 60:2567–75
118. Burgner J, Rucker DC, Gilbert HB, Swaney PJ, Russell PT, et al. 2014. A telerobotic system for transnasal surgery. *IEEE/ASME Trans. Mechatron.* 19:996–1006
119. Swaney PJ, Mahoney AW, Remirez AA, Lamers E, Hartley BI, et al. 2015. Tendons, concentric tubes, and a bevel tip: three steerable robots in one transoral lung access system. In *2015 IEEE International Conference on Robotics and Automation*, pp. 5378–83. Piscataway, NJ: IEEE
120. Wei W, Goldman R, Simaan N, Fine H, Chang S. 2007. Design and theoretical evaluation of micro-surgical manipulators for orbital manipulation and intraocular dexterity. In *2007 IEEE International Conference on Robotics and Automation*, pp. 3389–95. Piscataway, NJ: IEEE
121. Wei W, Goldman RE, Fine HF, Chang S, Simaan N. 2009. Performance evaluation for multi-arm manipulation of hollow suspended organs. *IEEE Trans. Robot.* 25:147–57
122. Lin FY, Bergeles C, Yang GZ. 2015. Biometry-based concentric tubes robot for vitreoretinal surgery. In *2015 IEEE International Conference on Engineering in Medicine and Biology*, pp. 5280–84. Piscataway, NJ: IEEE
123. Dwyer G, Chadebecq F, Amo MT, Bergeles C, Maneas E, et al. 2017. A continuum robot and control interface for surgical assist in fetoscopic interventions. *IEEE Robot. Autom. Lett.* 2:1656–63
124. Vandebroek T, Ourak M, Gruijthuijsen C, Javaux A, Legrand J, et al. 2019. Macro-micro multi-arm robot for single-port access surgery. In *2019 IEEE/RSJ International Conference on Intelligent Robots and Systems*, pp. 425–32. Piscataway, NJ: IEEE
125. Gosline AH, Vasilyev NV, Butler EJ, Folk C, Cohen A, et al. 2012. Percutaneous intracardiac beating-heart surgery using metal MEMS tissue approximation tools. *Int. J. Robot. Res.* 31:1081–93
126. Vasilyev NV, Gosline AH, Veeramani A, Wu MT, Schmitz GP, et al. 2014. Tissue removal inside the beating heart using a robotically delivered metal MEMS tool. *Int. J. Robot. Res.* 34:236–47
127. Amack S, Rox MF, Emerson M, Webster RJ, Alterovitz R, et al. 2019. Design and control of a compact modular robot for transbronchial lung biopsy. In *Medical Imaging 2019: Image-Guided Procedures, Robotic Interventions, and Modeling*, ed. B Fei, CA Linte, pap. 109510I. SPIE Proc. Vol. 1095. Bellingham, WA: SPIE
128. Hendrick RJ, Mitchell CR, Herrell SD, Webster RJ III. 2015. Hand-held transendoscopic robotic manipulators: a transurethral laser prostate surgery case study. *Int. J. Robot. Res.* 34:1559–72
129. Morimoto TK, Hawkes EW, Okamura AM. 2017. Design of a compact actuation and control system for flexible medical robots. *IEEE Robot. Autom. Lett.* 2:1579–85